

Flexible and Self-Healable Fluorescent Films with Tunable Emission via Solid-Phase Molecular Self-Assembly Design

Yanlei Xu, Shuting Wu, Hongjun Jin,* Ziyang Wu, Tongyue Wu, Wenning Cai, Wei Xiao, Qingrong Qian, Qinghua Chen,* and Yun Yan

Flexible luminescent materials are usually in the form of gels and films. Solid-state films have advantages in practical applications due to their long-term stability. However, the fabrication process by conventional methods remains laborious and unsustainable. Here, a facile and green route is reported for fabricating flexible luminescent films via an elegant solid-phase molecular self-assembly design. First, $\text{Eu}^{3+}/\text{Tb}^{3+}$ -based metallosupramolecular coordination polyelectrolytes (MEPEs) and tetraphenylethylene (TPE)-based MEPEs are designed with an antenna bis-ligands to get individual R, G, and B emission. Then, by repeatedly pressing the MEPEs-cetyltrimethylammonium bromide (CTAB) precipitates, obtained from their mixing aqueous solutions, R, G, and B emission films are obtained at room temperature, respectively. The emission color can be simply tuned by adjusting molar ratio of $\text{Eu}^{3+}:\text{Tb}^{3+}:\text{TPE}$. Notably, humidity-responsive white emission film is obtained when $\text{Eu}^{3+}:\text{Tb}^{3+}:\text{TPE} = 3:1:2.5$. Owing to the dynamic coordination and electrostatic interaction, which can be activated by hydrating water, these films can be facily reprocessed and self-healed with the aid of water at room temperature. It is hoped that this approach to fabricate flexible supramolecular luminescent films can be applied to design various advanced functional soft materials.

based luminescent materials (LnCs) are attracting increasing exploration due to their unique photoluminescent properties and dynamic metal-ligand coordination. LnCs possess large Stokes shifts, line-like emission, high quantum yield, high color purity and color-tunable emission, which make them fascinating for decades.^[11–13] Meanwhile, the dynamic nature of the lanthanide metal-ligand (Ln-L) coordination potentially endows LnCs with multi-stimulus responsiveness and self-healability, which leads LnCs more favorable in advanced luminescent materials.^[14–19]

Flexible LnCs luminescent materials with stimulus responsiveness and self-healability are generally in the form of gels and films, which are achieved by mixing lanthanide metal ions with small chelating ligands or chelating group grafted polymers. From the viewpoint of application, gels are limited by poor thermal and environmental stability, especially for hydrogels.^[20,21] Solid-state emission films show advantages in long-term stability during use, storage, and transport.

Luminescent films can be fabricated via layer-by-layer (LBL) assembly,^[22] electrodeposition technique,^[13] and solvent casting method.^[19] LBL and electrodeposition techniques are laborious and unsuitable for large-area fabrication. The solvent casting method is much more facile and commonly used to prepare films, but the substantial evaporation of organic solvents is tedious and energy-consuming. With the increasing demand for innovation in advanced luminescent materials, a facile and environmentally friendly route for fabricating flexible, self-healable, and stimulus-responsive luminescent films is therefore urgently needed.

Molecular self-assembly represents a powerful tool to fabricate functional soft materials across basic science, technology, and nature.^[23–25] As an important complement to traditional solution assembly leading to suspensions and gels, we recently developed a solid-phase molecular self-assembly (SPMSA) strategy to construct supramolecular films by mildly pressing the wet precipitates of oppositely charged polyelectrolytes (PEs) and surfactants (SAa) at room temperature.^[26–29] Such room-temperature pressing strategy provides a facile and green way to fabricate bulk supramolecular films. Thus, in this work, we report a flexible and self-healable fluorescent film with tunable

1. Introduction

Flexible and stretchable luminescent materials have displayed promising applications in flexible display,^[1,2] soft robot,^[3,4] electronic skin,^[5,6] intelligent sensing/detection,^[7,8] and information encryption.^[9,10] Wherein, lanthanide coordination complex-

Y. Xu, S. Wu, H. Jin, Z. Wu, W. Cai, W. Xiao, Q. Qian, Q. Chen
Engineering Research Center of Polymer Green Recycling of Ministry of Education

College of Environmental and Resource Sciences
College of Carbon Neutral Modern Industry
Fujian Normal University
Fuzhou, Fujian 350007, China

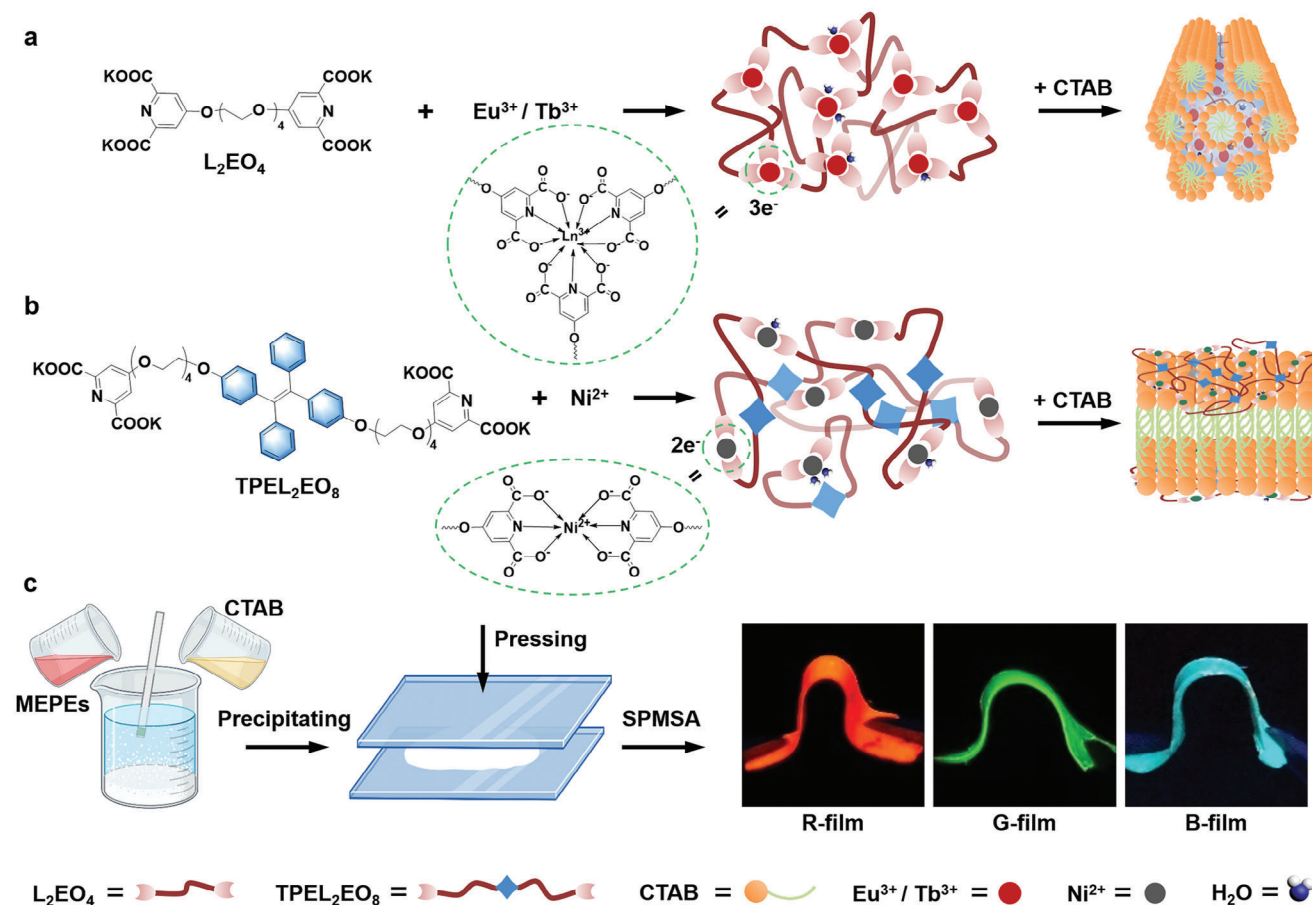
E-mail: hongjunjin@fjnu.edu.cn; cqhuar@fjnu.edu.cn

T. Wu, Y. Yan

Beijing National Laboratory for Molecular Sciences (BNLMS)
College of Chemistry and Molecular Engineering
Peking University
Beijing 100871, China

The ORCID identification number(s) for the author(s) of this article can be found under <https://doi.org/10.1002/adom.202402258>

DOI: 10.1002/adom.202402258



Scheme 1. a) Illustration of the formation of $\text{L}_2\text{EO}_4\text{-Eu}^{3+}/\text{Tb}^{3+}$ MEPEs and the hexagonal mesostructure formed in $\text{L}_2\text{EO}_4\text{-Eu}^{3+}/\text{Tb}^{3+}\text{-CTAB}$ films. b) Illustration of the formation of $\text{TPEL}_2\text{EO}_8\text{-Ni}^{2+}$ MEPEs and the lamellar mesostructure formed in $\text{TPEL}_2\text{EO}_8\text{-Ni}^{2+}\text{-CTAB}$ films. c) Illustration of the solid phase molecular self-assembly (SPMSA) for preparing the flexible RGB emission films based on MEPEs-CTAB.

emission and humidity responsiveness via a delicate SPMSA design. It is well-known that appropriate bis- or tris-ligands connect metal ions to form metallosupramolecular coordination polyelectrolytes (MEPEs),^[30–34] which can further form complexes with surfactant and polyelectrolyte via electrostatic interactions.^[35,36] Besides, the lanthanide ions suffer from weak light absorption owing to the f-f transitions, leading to a very weak emission when directly excite the metal ions. By coordinating with appropriate antenna groups, the emission can be greatly sensitized via energy transfer from ligands to metal ions, known as “antenna effect.”^[22,37–40] Hence, a bis-ligand 1,11-bis(2,6-dicarboxypyridin-4-yloxy)-3,6,9-tri-oxaundecane (L_2EO_4) is used in this work to form MEPEs with Eu^{3+} and Tb^{3+} , which intensely emit red (R) and green (G) emission by coordinating with the antenna group of pyridine dicarboxylate. In addition, to obtain full-color tunable fluorescence, a blue (B) emission MEPE is designed with a tetraphenylethylene (TPE) containing bis-ligand (TPEL_2EO_8) and nonemissive Ni^{2+} . These R, G, and B emission MEPEs, which are all negatively charged, can electrostatically interact with cationic surfactant cetyltrimethylammonium bromide (CTAB) in aqueous solution to form precipitates. By gently pressing these precipitates, flexible supramolecular fluorescent films are gradually formed, as illustrated in **Scheme 1**. Based on the RGB color

model, the emission color can be delicately tuned by simply adjusting the stoichiometry of RGB emission components. It is worth noting that white emission film (W-film) is obtained when $\text{Eu}^{3+} : \text{Tb}^{3+} : \text{TPE} = 3 : 1 : 2.5$. Owing to the dynamic nature of coordination, the fluorescent films show humidity responsiveness. With increasing relative humidity (RH), the fluorescent intensity of the R, G, and B-films reduced gradually and the W-film displayed a distinct color change. Meanwhile, driven by the reversible coordination and electrostatic interaction, which can be greatly activated by water, these films can be facily reprocessed and self-healed with the aid of water at room temperature. We anticipate the present work providing a new strategy to construct flexible and self-healable luminescent supramolecular films and bringing a new perspective for designing advanced soft materials.

2. Results and Discussion

The preparation of MEPEs-SAa fluorescent films was inspired by our recently developed SPMSA strategy, by which bulk supramolecular films can be facily fabricated with oppositely charged PEs and SAa.^[26–29] MEPEs are similar to PEs due to the chain/network structure and the charged coordination centers

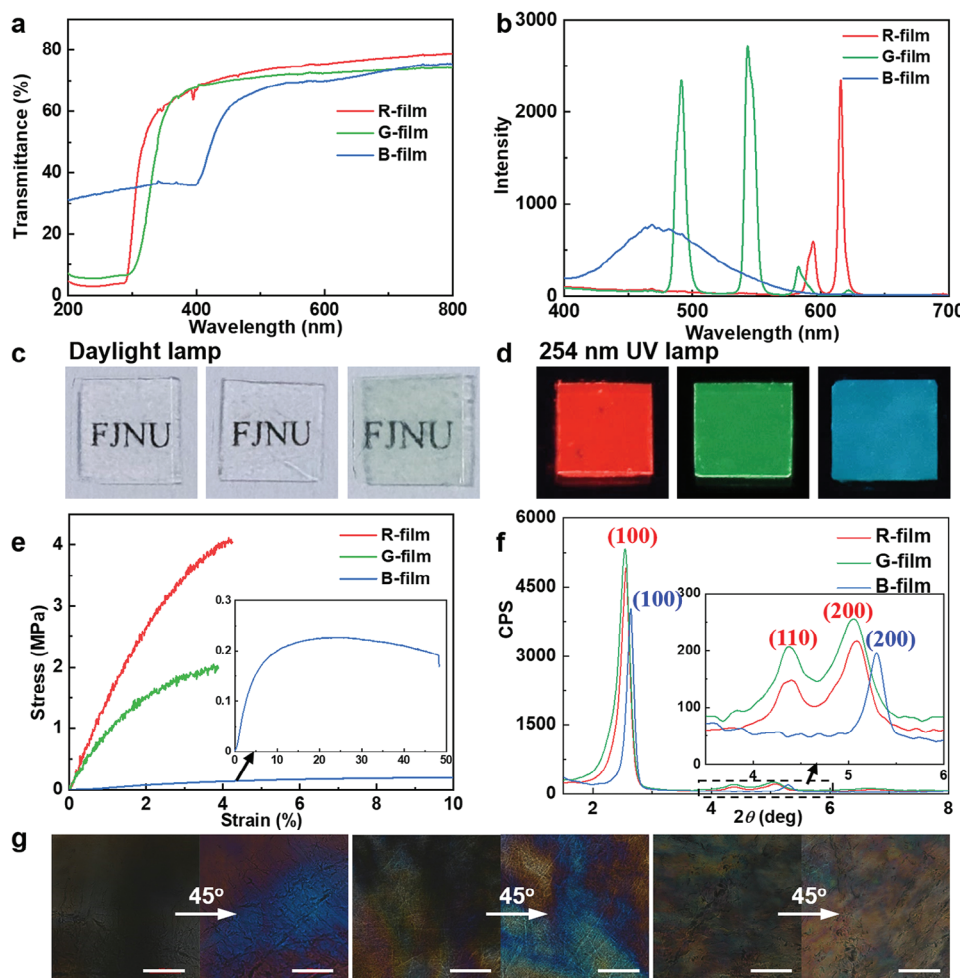


Figure 1. a) UV-vis transmission spectra of the RGB-films. b) Fluorescence spectra ($\lambda_{\text{ex}} = 254$ nm) of the RGB-films. c) Optical images of the RGB-films under daylight lamp. d) Optical images of the RGB-films under 254 nm UV lamp. e) Stress-strain curves of the RGB-films. f) XRD patterns of the RGB-films. g) The birefringence of the RGB-films observed by POM, respectively. Scale bar 100 μm .

in the network. Thus, appropriate MEPEs and SAa are expected to successfully construct supramolecular films through SPMSA. Meanwhile, for the purpose of full-color emission, individual R, G and B emission MEPEs were designed in this work. The R and G emission MEPEs were constructed with nonemissive bis-ligand L_2EO_4 and luminescent lanthanide metal ions Eu^{3+} and Tb^{3+} at molar ratio of $\text{Ln}^{3+} : \text{L}_2\text{EO}_4 = 2:3$, respectively (Scheme 1a). The B emission MEPE was formed with nonemissive transition metal ion Ni^{2+} and TPE containing bis-ligand TPEL_2EO_8 at molar ratio of $\text{Ni}^{2+} : \text{TPEL}_2\text{EO}_8 = 1:1$ (Scheme 1b). Fluorescent emission was negligible for aqueous solutions of $\text{Eu}(\text{NO}_3)_3$, $\text{Tb}(\text{NO}_3)_3$, and TPEL_2EO_8 at the concentrations used in our experiments. Once mixing the corresponding metal ions and bis-ligands, strong fluorescence was observed (Figure S1, Supporting Information), suggesting the successful formation of MEPEs. The fluorescent emission was derived from the “antenna effect” for Ln^{3+} -based MEPEs and aggregation-induced emission for TPE-based MEPE. The fluorescent quantum yields at 254 nm excitation were 9.48%, 12.09%, and 0.47% for the RGB emission MEPEs solutions, respectively. All of the above MEPEs were neg-

atively charged according to the coordination mode.^[22,37] Upon adding the oppositely charged surfactant CTAB at charge balancing ratio, precipitates occurred immediately. By repeatedly pressing the wet precipitates at room temperature, self-supporting and flexible RGB emission fluorescent films gradually formed within 20 min, which were denoted by $\text{L}_2\text{EO}_4\text{-Eu}^{3+}\text{-CTAB}$ (R-film), $\text{L}_2\text{EO}_4\text{-Tb}^{3+}\text{-CTAB}$ (G-film) and $\text{TPEL}_2\text{EO}_8\text{-Ni}^{2+}\text{-CTAB}$ (B-film), respectively (Scheme 1c).

UV-vis spectra show all the fluorescent films are transparent in the visible range and strongly absorb UV light (Figure 1a). When excited by 254 nm UV light, all the films exhibited intense fluorescent emission shown in Figure 1b. The R-film shows the characteristic emission peaks at 594 and 616 nm, corresponding to $^5\text{D}_0 - ^7\text{F}_1$ and $^5\text{D}_0 - ^7\text{F}_2$ transitions of europium, respectively. Analogously, the G-film displays the characteristic emission peaks at 491, 543, 583, and 622 nm, corresponding to $^5\text{D}_4 - ^7\text{F}_6$, $^5\text{D}_4 - ^7\text{F}_5$, $^5\text{D}_4 - ^7\text{F}_4$, and $^5\text{D}_4 - ^7\text{F}_3$ transitions of terbium, respectively. The B-film shows a typical broad peak ≈ 475 nm because the emitting is derived from the aggregation-induced emission of TPE group. The fluorescence quantum yields were

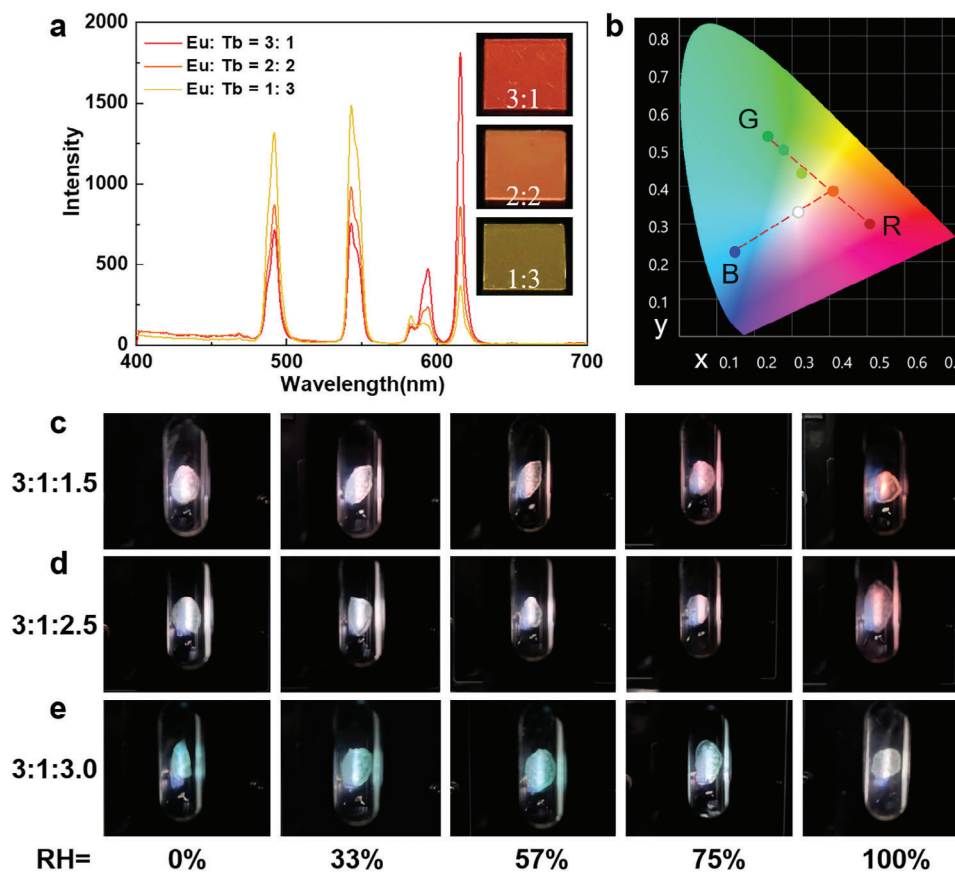


Figure 2. a) Fluorescence spectra ($\lambda_{\text{ex}} = 254 \text{ nm}$) of the luminescent films with $\text{Eu}^{3+}:\text{Tb}^{3+} = 3:1$, $2:2$ and $1:3$, respectively. b) CIE 1931 diagram with coordinates of the RGB-films and the films in (a). c–e) Optical images of the luminescent films with $\text{Eu}^{3+}:\text{Tb}^{3+}:\text{TPE} =$ (c) $3:1:1.5$, (d) $3:1:2.5$ and (e) $3:1:3.0$, respectively ($\lambda_{\text{ex}} = 254 \text{ nm}$).

all greatly improved to 74.33%, 22.45%, and 1.67%, respectively, compared to the MEPEs solutions. Figure 1c,d are optical images of the RGB-films under daylight lamp and 254 nm UV lamp, respectively. Mechanical test reveals the tensile breaking strengths are 4.2, 2.0, and 0.2 MPa, and the Young's moduli are 133, 92, and 3.4 MPa, respectively, for the dry RGB-films (Figure 1e). The much larger breaking strain for B-film can be ascribed to the longer flexible EO chain, providing more chain winding and energy dissipation mechanisms for strain. X-ray diffraction (XRD) patterns (Figure 1f) manifest the CTAB molecules in the R-film and G-film pack into hexagonal mesostructure, owing to the appearance of characteristic (100), (110) and (200) diffraction peaks with spacing ratio of $1:\sqrt{3}:\sqrt{4}$. Only (100) and (200) diffraction peaks with spacing ratio of 1:2 occur in the B-film, indicating the CTAB molecules aggregates into lamellar phase. It is worth mentioning that all the corresponding d values for the (100) diffraction peaks are $\approx 3.4 \text{ nm}$, which are shorter than twice the extending length of CTAB molecules (4.2 nm, Figure S2a, Supporting Information), indicating the alkyl chains of CTAB are highly staggered. Besides, the extending length of TPE₂EO₈ bisligand is $\approx 4.8 \text{ nm}$ (Figure S2b, Supporting Information). In order to rule out the formation of TPE₂EO₈ lamella, CTAB was replaced by tetradecyltrimethylammonium bromide (TTAB) and dodecyltrimethylammonium bromide (DTAB). The lamellar pe-

riod decreased from 3.35 to 3.20 nm and 3.05 nm with the decreasing of alkyl chain length (Figure S2c, Supporting Information). Therefore, the molecular arrangement in the RGB-films can be illustrated as shown in Scheme 1a,b. In addition, all the RGB-films displayed strong birefringence under polarized optical microscopy (POM), which also confirmed the formation of anisotropic structures (Figure 1e).

According to the RGB color model, the full spectrum of emission can be obtained by mixing the primary colors of R, G, and B light, together in various proportions. For instance, when the molar ratio of Eu^{3+} and Tb^{3+} varied from 3:1 to 1:3, the emission color of the obtained films gradually changed from nazarat to yellow-green (Figure 2a). This color change can also be shown in the CIE 1931 diagram (Figure 2b), according to the fluorescent spectra. The CIE coordinates shift linearly from $\text{Eu}^{3+}:\text{Tb}^{3+} = 4:0$ to $0:4$ (Figure 2d; Table S1 and Figure S3, Supporting Information). The fitting linear equation is $y = 0.71 - 0.71x$ ($R^2 = 0.97$, line 1). The linear equation of the CIE coordinates for the blue emission and theoretical white emission is $y = 0.12 + 0.63x$ (line 2), which intersects line 1 at (0.41, 0.38), coinciding with the coordinate (0.41, 0.39) of $\text{Eu}^{3+}:\text{Tb}^{3+} = 3:1$. Thus, white emission can be obtained theoretically by adding appropriate amount of TPE to $\text{Eu}^{3+}:\text{Tb}^{3+} = 3:1$. Figure 2c–e shows the optical images of the luminescent films with different molar ratio of $\text{Eu}^{3+}:\text{Tb}^{3+}$:

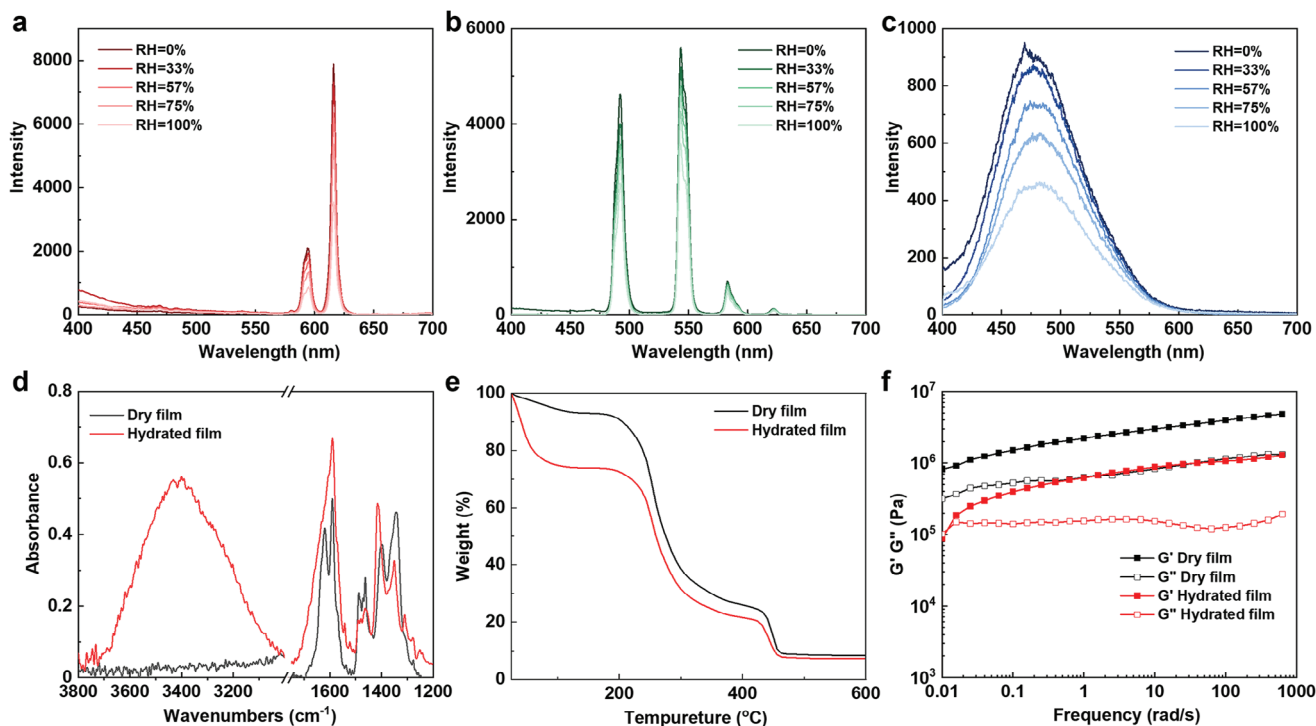


Figure 3. Fluorescence spectra ($\lambda_{\text{ex}} = 254 \text{ nm}$) of a) R-film, b) G-film, and c) B-film under RH of 0, 33%, 57%, 75%, and 100%, respectively. All the films were placed in the sealed container with constant RH for at least one day before tests. d) FT-IR spectra, e) TGA curves, and f) Frequency sweeps showing the storage moduli (G' , filled data points) and loss moduli (G'' , open data point) of the dry and hydrated R-film.

TPE. By steadily increasing the proportion of TPE from 3:1:1.5 to 3:1:3.0, the emission color of the dry films (relative humidity, RH = 0%) changed from reddish white to blue. And when the molar ratio was 3:1:2.5, W-film was also obtained. Surprisingly, the emission color of these composite films was stimulus responsive to RH. The reddish white film of 3:1:1.5 gradually turned red with the increasing RH (Figure 2c). The 3:1:2.5 film displayed white emission at 0–57% RH, but also turned red under higher RH (Figure 2d). The blue emission 3:1:3.0 film gradually faded and became white at RH = 100% (Figure 2e). Meanwhile, **Figure 3a–c** shows that all the fluorescent intensity of the R, G and B emission films reduced gradually with the increasing RH. And the R, G, B emission faded 34%, 45% and 48% from RH = 0 to 100%, respectively, according to the integral area of the spectrum. Thus, although the color fade was unobservable by naked eyes of the individual R, G and B films, the color of composite films with near-white emission were very sensitive to humidity, as the G and B emissive elements were more sensitive to humidity and faded more sharply.

This humidity responsiveness of emission color was derived from the strong hygroscopicity of MEPE-SAA films, similar to our previously reported PE-SAA films.^[26–29] The decrease in fluorescence intensity with RH provided an indication of increasing amount of hydrating water on $\text{Eu}^{3+}/\text{Tb}^{3+}$ and a looser environment for TPE. Taking R-film for example, when soaked in water, it quickly hydrated to equilibrium within 2 min (Figure S4a, Supporting Information). And the fluorescence markedly decreased by 76% (Figure S4b, Supporting Information), manifesting the europium ions were highly hydrated. The strong stretching vi-

bration at $\approx 3400 \text{ cm}^{-1}$ of O-H, shown in Fourier transform infrared (FT-IR) spectra (**Figure 4d**), also confirmed the existence of abundant water in the hydrated film. Although the asymmetric stretching vibration of carbonyl was overlapped by the bending vibration of O-H at $\approx 1600 \text{ cm}^{-1}$, the symmetrical stretching vibration of carbonyl at $\approx 1400 \text{ cm}^{-1}$ evidently blue shifted, indicating the carboxyl groups were also hydrated. Thermogravimetric analysis (TGA) shows the water contents for the dry and hydrated R-films are 7% and 26%, respectively (Figure 3e). Water molecules are supposed to bind to the polar groups around the coordination center including carboxyl groups, quaternary ammonium groups, and metal ions. Each coordination center bound 7.5 and 34.8 water molecules in the dry and hydrated R-films according to the TGA results. These water molecules weakened the coordination bindings between carboxyl groups and metal ions, as well as the electrostatic interactions between MEPEs and CTAB, leading to remarkable decrease in fluorescent emission and also mechanical strength. The hydrated films became much more flexible, which was further clarified by the rheological test. Both G' representing elasticity and G'' representing viscosity was significantly decreased after hydrated (Figure 3f).

The hydroplasticity can be also verified by the stress–strain curves. The tensile breaking strength notably decreased after hydrating, while the breaking strain increased (Figure 4a, black line), compared to the dry film (Figure 1e, red line). Owing to this hydroplasticity, the reversibility of coordinate/ionic bonds and the mobility of molecular rearrangement can be significantly enhanced when wetted with water. Thus, these films can be facily reprocessed and self-healed multiple times with the aid of water

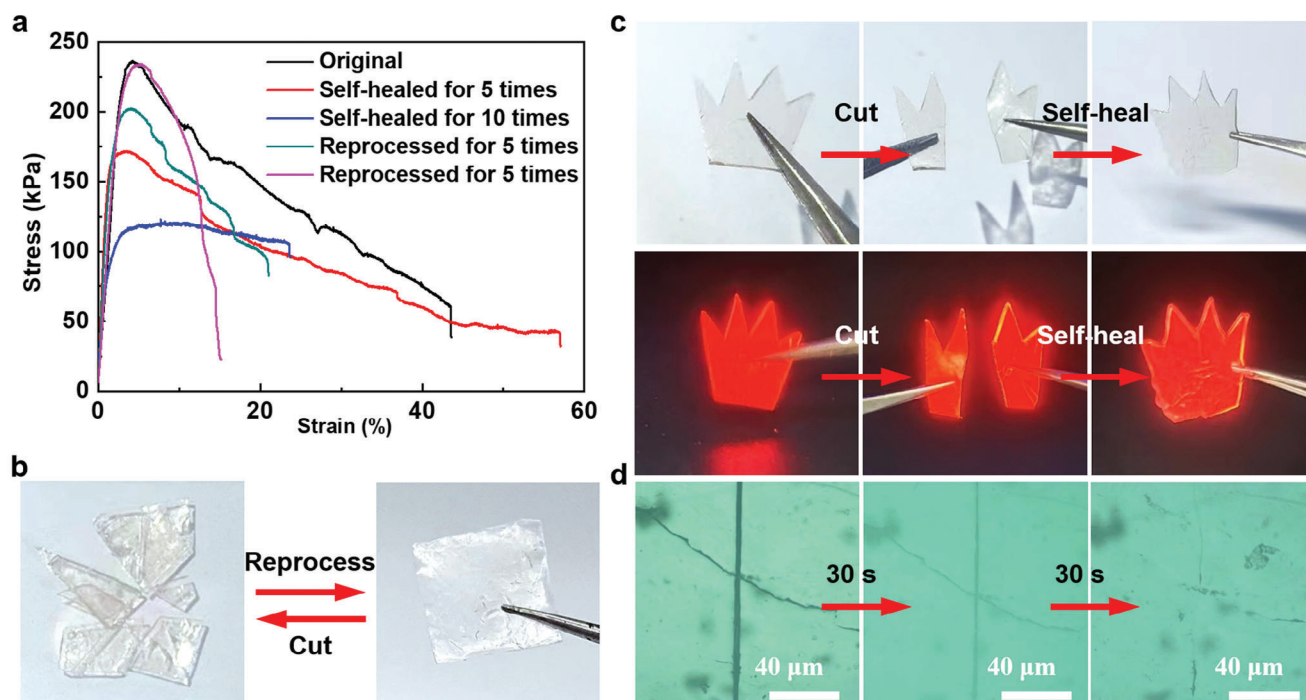


Figure 4. a) Stress–strain curves of the original, self-healed and reprocessed R-films. All the films were fully hydrated. b) Demonstration of the reprocessing of R-film. c) Demonstration of the self-healing of R-film. d) Optical microscopic images showing the fracture self-healing within 1 min at room temperature.

at room temperature, which is illustrated by R-film as an example in Figure 4. When the films were cut into small pieces, they can be reprocessed into new ones by wetting with drops of water and then repeatedly pressing at room temperature (Figure 4b). The regenerated wet films retained comparable mechanical properties to the original films as demonstrated by the stress–strain tests (Figure 4a). Meanwhile, when the cut films were placed in contact and pressed together slightly, the cut pieces connected within 1 min (Figure 4c). The rapid self-healing of the damaged section can be seen using optical microscope (Figure 4d). The stress–strain tests also show the considerable recovery of mechanical properties after self-healing (Figure 4a).

3. Conclusion

In summary, we report a facile and green strategy to fabricate emission tunable supramolecular luminescent films via an elegant solid-phase molecular self-assembly (SPMSA) design. First, individual R, G and B emission metallosupramolecular coordination polyelectrolytes (MEPEs) were elaborately constructed with $\text{Eu}^{3+}/\text{Tb}^{3+}$ -based MEPEs and TPE-based MEPEs. Then, RGB emission MEPEs-CTAB films were respectively obtained at room temperature by repeatedly pressing the MEPEs-CTAB precipitates, forming by mixing their aqueous solutions. The emission color can be simply tuned by adjusting the molar ratio of $\text{Eu}^{3+}:\text{Tb}^{3+}:\text{TPE}$. Owing to the dynamic coordination, the fluorescent films show humidity responsiveness. Furthermore, these films can be facily reprocessed and self-healed with the assist of water at room temperature, because of the water-activated reversible coordination and electrostatic interaction. Thus, these films are

aqueous processable and self-healable, which are highly sustainable and in line with the purpose of green chemistry.

4. Experimental Section

Fabrication of $\text{L}_2\text{EO}_4\text{-Eu}^{3+}/\text{Tb}^{3+}$ -CTAB Film: L_2EO_4 , $\text{Eu}(\text{NO}_3)_3/\text{Tb}(\text{NO}_3)_3$ and CTAB were first dissolved in water to from stock solutions at concentration of 10, 6.67, and 20 mM, respectively. Red/green emission metallosupramolecular coordination polyelectrolytes (MEPEs) were formed immediately upon mixing L_2EO_4 and $\text{Eu}^{3+}/\text{Tb}^{3+}$ solutions at a molar ratio of 3:2. Then white precipitates were formed when CTAB solution was added to the MEPEs solution at charge balancing ratio, and the precipitates were separated and collected through centrifugation. The collected precipitates were condensed by finger pressing with pressure ≈ 0.5 MPa under ambient environment, which gradually transformed to a transparent film within 30 min at room temperature. The fabricating process is shown in Video S1 (Supporting Information).

Fabrication of $\text{TPEL}_2\text{EO}_8\text{-Ni}^{2+}$ -CTAB Film: TPEL_2EO_8 , $\text{Ni}(\text{NO}_3)_2$, and CTAB were first dissolved in water from stock solutions at concentrations of 10, 10, and 20 mM, respectively. Blue emission MEPEs were formed immediately upon mixing TPEL_2EO_8 and Ni^{2+} solutions at a molar ratio of 1:1. Then green precipitates were formed when CTAB solution was added to the MEPEs solution at charge balancing ratio. The $\text{TPEL}_2(\text{EO})_4\text{-Ni}^{2+}$ -CTAB film was obtained via the same fabricating process as above.

Fabrication of Composite Emission Films: First, red, green, and blue emission MEPEs were respectively prepared as above. The concentrations of these stocking MEPEs were denoted by the molar concentration of the corresponding luminous element, which was 3.33 mM for Eu^{3+} , 3.33 mM for Tb^{3+} , and 5 mM for TPE core, respectively. Then these MEPEs were mixed at different molar ratio for various emission colors. Finally, CTAB solution was added to the MEPEs solution at a charge balancing ratio to get precipitates. The composite emission films were obtained via the

same fabricating process as above. For example, the white emission film was prepared as follows: 3 mL of red emission MEPE, 1 mL of green emission MEPE, and 1.667 mL of blue emission MEPE were mixed first. Then 2.833 mL of 20 mM CTAB was added to balance the negative charges of MEPEs and forming precipitates. The precipitates were separated and collected through centrifugation, and then condensed by finger pressing with pressure ≈ 0.5 MPa under ambient environment, which gradually transformed to white emission film within 30 min at room temperature. Thus, the composition of this film was denoted as $\text{Eu}^{3+}:\text{Tb}^{3+}:\text{TPE} = (3 \text{ mL} \times 3.33 \text{ mM}) : (1 \text{ mL} \times 3.33 \text{ mM}) : (1.667 \text{ mL} \times 5 \text{ mM}) = 3:1:2.5$.^[41,42]

Relative Humidity Control: To control the relative humidity, anhydrous calcium chloride (RH = 0%), saturated salt solutions (RH = 33–75%), and pure water of desired relative humidity were prepared and allowed to equilibrate in a closed container at room temperature: 0% RH CaCl_2 , 33% RH MgCl_2 , 57% RH NaBr, 75% RH NaCl, 100% RH H_2O . The films were placed in the sealed container for at least 1 day before other tests.

Supporting Information

Supporting Information is available from the Wiley Online Library or from the author.

Acknowledgements

Y.X. and S.W. contributed equally to this work. This work was financially supported by the National Natural Science Foundation of China (NSFC 22202044) and the Natural Science Foundation of Fujian Province, China (2023J05036).

Conflict of Interest

The authors declare no conflict of interest.

Data Availability Statement

The data that support the findings of this study are available from the corresponding author upon reasonable request.

Keywords

emission tuning, fluorescent film, processing, self-healing, solid-phase molecular self-assembly

Received: August 21, 2024
Revised: October 21, 2024
Published online: November 18, 2024

- [1] X. Shi, Y. Zuo, P. Zhai, J. Shen, Y. Yang, Z. Gao, M. Liao, J. Wu, J. Wang, X. Xu, Q. Tong, B. Zhang, B. Wang, X. Sun, L. Zhang, Q. Pei, D. Jin, P. Chen, H. Peng, *Nature* **2021**, *591*, 240.
- [2] J.-H. Oh, J.-W. Park, *ACS Appl. Mater. Interfaces* **2023**, *15*, 33784.
- [3] P. Zhang, I. M. Lei, G. Chen, J. Lin, X. Chen, J. Zhang, C. Cai, X. Liang, J. Liu, *Nat. Commun.* **2022**, *13*, 4775.
- [4] Z. Wang, J. Bao, R. Huang, C. Song, C. Shen, J. Sun, R. Lan, L. Zhang, H. Yang, *Sci. China Mater.* **2023**, *66*, 2445.
- [5] D. Son, J. Kang, O. Vardoulis, Y. Kim, N. Matsuhisa, J. Y. Oh, J. W. F. To, J. Mun, T. Katsumata, Y. Liu, A. F. McGuire, M. Krason, F. Molina-Lopez, J. Ham, U. Kraft, Y. Lee, Y. Yun, J. B. H. Tok, Z. Bao, *Nat. Nanotechnol.* **2018**, *13*, 1057.
- [6] H. Kim, J. Choi, K. K. Kim, P. Won, S. Hong, S. H. Ko, *Nat. Commun.* **2021**, *12*, 4658.
- [7] M. Xie, Y. Che, K. Liu, L. Jiang, L. Xu, R. Xue, M. Drechsler, J. Huang, B. Z. Tang, Y. Yan, *Adv. Funct. Mater.* **2018**, *28*, 1803370.
- [8] H. Nawaz, S. Chen, X. Zhang, X. Li, T. You, J. Zhang, F. Xu, *ACS Nano* **2023**, *17*, 3996.
- [9] N. Gan, X. Zou, Z. Qian, A. Lv, L. Wang, H. Ma, H.-J. Qian, L. Gu, Z. An, W. Huang, *Nat. Commun.* **2024**, *15*, 4113.
- [10] J. Huang, Y. Jiang, Q. Chen, H. Xie, S. Zhou, *Nat. Commun.* **2023**, *14*, 7131.
- [11] K. Binnemans, *Chem. Rev.* **2009**, *109*, 4283.
- [12] P. Li, H. Li, *Coord. Chem. Rev.* **2021**, *441*, 213988.
- [13] H. Liu, T. Chu, Z. Rao, S. Wang, Y. Yang, W. T. Wong, *Adv. Opt. Mater.* **2015**, *3*, 1545.
- [14] P. Chen, Q. Li, S. Grindy, N. Holten-Andersen, *J. Am. Chem. Soc.* **2015**, *137*, 11590.
- [15] G. Weng, S. Thanneeru, J. He, *Adv. Mater.* **2018**, *30*, 1706526.
- [16] J. Yang, T. Wang, R. Guo, D. Yao, W. Guo, S. Liu, Z. Li, Y. Wang, H. Li, *ACS Appl. Mater. Interfaces* **2020**, *12*, 54026.
- [17] J. Yang, Z. Zhang, Y. Yan, S. Liu, Z. Li, Y. Wang, H. Li, *ACS Appl. Mater. Interfaces* **2020**, *12*, 13239.
- [18] J. Yang, D. Zhao, D. Yao, Y. Wang, H. Li, *Chem. Eng. J.* **2021**, *426*, 131595.
- [19] D. Zhao, J. Yang, X. Tian, J. Wei, Q. Li, Y. Wang, *Chem. Eng. J.* **2022**, *434*, 134806.
- [20] F. Xin, Q. Lyu, *Gels* **2023**, *9*, 7.
- [21] M. A. Kuzina, D. D. Kartsev, A. V. Stratonovich, P. A. Levkin, *Adv. Funct. Mater.* **2023**, *33*, 2301421.
- [22] J. Yang, Y. Yan, Y. Hui, J. Huang, *J. Mater. Chem. C* **2017**, *5*, 5083.
- [23] H. Jin, Z. Wu, W. Lin, Y. Chen, J. Zhang, R. Zheng, H. Wei, Q. Chen, Q. Qian, J. Huang, J. Zhang, Y. Yan, *Small* **2023**, *19*, 2300688.
- [24] L. Jiang, J. W. de Folter, J. Huang, A. P. Philipse, W. K. Kegel, A. V. Petukhov, *Angew. Chem. Int. Ed.* **2013**, *52*, 3364.
- [25] J. Gao, J. Zhan, Z. Yang, *Adv. Mater.* **2020**, *32*, 1805798.
- [26] H. Jin, M. Xie, W. Wang, L. Jiang, W. Chang, Y. Sun, L. Xu, S. Zang, J. Huang, Y. Yan, L. Jiang, *CCS Chem.* **2020**, *2*, 98.
- [27] H. Jin, C. Ma, W. Wang, Y. Cai, J. Qi, T. Wu, P. Liao, H. Li, Q. Zeng, M. Xie, J. Huang, Y. Yan, *ACS Mater. Lett.* **2021**, *4*, 145.
- [28] P. Liao, S. Zang, T. Wu, H. Jin, W. Wang, J. Huang, B. Z. Tang, Y. Yan, *Nat. Commun.* **2021**, *12*, 5496.
- [29] H. Jin, W. Lin, Z. Wu, X. Cheng, X. Chen, Y. Fan, W. Xiao, J. Huang, Q. Qian, Q. Chen, Y. Yan, *Adv. Mater.* **2023**, *35*, 2207688.
- [30] M. Burnworth, L. Tang, J. Kumpfer, A. Duncan, F. Beyer, G. Fiore, S. Rowan, C. Weder, *Nature* **2011**, *472*, 334.
- [31] F. Han, M. Higuchi, D. Kurth, *J. Am. Chem. Soc.* **2008**, *130*, 2073.
- [32] L. Xu, L. Jiang, M. Drechsler, Y. Sun, Z. Liu, J. Huang, B. Z. Tang, Z. Li, M. A. Stuart, Y. Yan, *J. Am. Chem. Soc.* **2014**, *136*, 1942.
- [33] Y. Yan, N. A. Besseling, A. de Keizer, A. T. Marcellis, M. Drechsler, M. A. Cohen Stuart, *Angew. Chem., Int. Ed.* **2007**, *46*, 1807.
- [34] D. W. R. Balkenende, S. Coulibaly, S. Balog, Y. C. Simon, G. L. Fiore, C. Weder, *J. Am. Chem. Soc.* **2014**, *136*, 10493.
- [35] D. Kurth, A. Meister, A. Thunemann, G. Forster, *Langmuir* **2003**, *19*, 4055.
- [36] D. G. Kurth, R. Osterhout, *Langmuir* **1999**, *15*, 4842.
- [37] T. Wu, M. Xie, J. Huang, Y. Yan, *ACS Appl. Mater. Interfaces* **2020**, *12*, 39578.
- [38] J. Wang, S. Sun, B. Wu, L. Hou, P. Ding, X. Guo, M. A. Cohen Stuart, J. Wang, *Macromolecules* **2019**, *52*, 8643.
- [39] L. Xu, L. Feng, Y. Han, Y. Jing, Z. Xian, Z. Liu, J. Huang, Y. Yan, *Soft Matter* **2014**, *10*, 4686.
- [40] Y. Cui, Y. Yue, G. Qian, B. Chen, *Chem. Rev.* **2012**, *112*, 1126.
- [41] J. C. Tellis, C. A. Strulson, M. M. Myers, K. A. Kneas, *Anal. Chem.* **2011**, *83*, 928.
- [42] L. Greenspan, *J. Res. Natl. Bur. Stand.-A. Phys. Chem.* **1977**, *81*, 89.